Nuclear Engineering and Technology 52 (2020) 2196–2203

Contents lists available at ScienceDirect

Nuclear Engineering and Technology

journal homepage: www.elsevier.com/locate/net

Original Article

A *dryout* mechanism model for rectangular narrow channels at high pressure conditions

Gongle Song [a], Yu Liang [a], Rulei Sun [a], Dalin Zhang [a, *], Jian Deng [b, **], G.H. Su [a], Wenxi Tian [a], Suizheng Qiu [a]

[a] School of Nuclear Science and Technology, Shaanxi Key Laboratory of Advanced Nuclear Energy and Technology, State Key Laboratory of Multiphase Flow in Power Engineering, Xi'an Jiaotong University, Xi'an, 710049, China
[b] Science and Technology on Reactor System Design Technology Laboratory, Nuclear Power Institute of China, Chengdu, 610041, China

ARTICLE INFO

Article history:
Received 26 December 2019
Received in revised form
19 February 2020
Accepted 18 March 2020
Available online 19 March 2020

Keywords:
Dryout
CHF
Kelvin-Helmholtz instability
Mechanism model
Rectangular narrow channels

ABSTRACT

A *dryout* mechanism model for rectangular narrow channels at high pressure conditions is developed by assuming that the Kelvin–Helmholtz instability triggered the occurrence of *dryout*. This model combines the advantages of theoretical analysis and empirical correlation. The unknown coefficients in the theoretical derivation are supported by the experimental data. Meanwhile, the decisive restriction of the experimental conditions on the applicability of the empirical correlation is avoided. The expression of vapor phase velocity at the time of *dryout* is derived, and the empirical correlation of liquid film thickness is introduced. Since the CHF value obtained from the liquid film thickness should be the same as the value obtained from the Kelvin–Helmholtz critical stability under the same condition, the convergent CHF value is obtained by iteratively calculating. Comparing with the experimental data under the pressure of 6.89–13.79 MPa, the average error of the model is −15.4% with the 95% confidence interval [-20.5%, −10.4%]. And the pressure has a decisive influence on the prediction accuracy of this model. Compared with the existing *dryout* code, the calculation speed of this model is faster, and the calculation accuracy is improved. This model, with great portability, could be applied to different objects and working conditions by changing the expression of the vapor phase velocity when the dryout phenomenon is triggered and the calculation formula of the liquid film.

1. Introduction

The plate type fuel element has the advantages of compact structure, high power per unit volume, low central temperature, high burnup, low heat storage and good safety. It is an advanced design structure of the new integrated pressurized water reactor core. The coolant flow channel of the plate type fuel element is a typical rectangular narrow channel, which has compact structure, small temperature difference of heat transfer, simple surface processing, smoothness of heat transfer surface. Besides, it is not easy to produce impurities and pollute the heat transfer surface to deteriorate heat transfer with the high-speed fluid. Due to the above characteristics, the rectangular narrow channel is widely used in the fields of chemical, nuclear energy, electronic device cooling, refrigeration and others. The research on the thermal hydraulic properties of rectangular narrow channels has become a hot research topic [1,2].

Critical heat flux (CHF) is the most important thermal hydraulic limit parameter to ensure reactor core safety. When the critical boiling occurs, the flow boiling mechanism of the coolant changes, the heat transfer coefficient decreases, and the heat transfer on the surface of the nuclear fuel element deteriorates. In severe cases, the fuel element can be burned and even cause the radioactive leakage. It is generally believed that in region of the annular flow, CHF is caused by liquid film drying, and the CHF model established accordingly is called dryout model. Due to the wide range of quality (about 0.1–1.0) corresponding to the annular flow pattern, dryout is of great significance for the safety analysis and transient process of boiling water reactors and pressurized water reactors. In recent years, the dryout model has received much attention [3,4].

In rectangular narrow channels, bubble growth is limited, and

* Corresponding author.
** Corresponding author.
E-mail addresses: dlzhang@mail.xjtu.edu.cn (D. Zhang), dengjian_npic@163.com (J. Deng).

https://doi.org/10.1016/j.net.2020.03.018

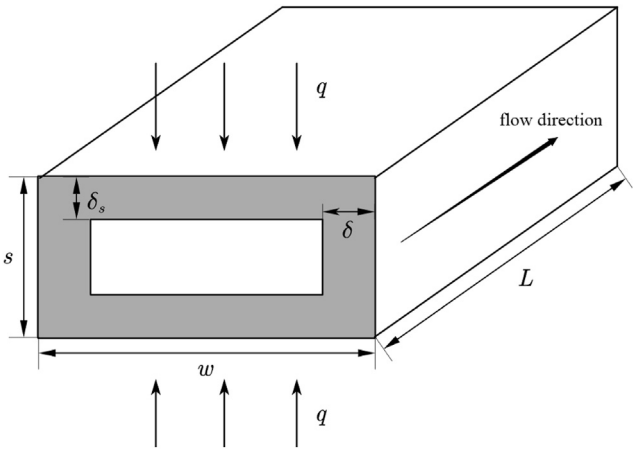

Fig. 1. Schematic diagram of rectangular channel structure.

thus the characteristic of the critical heat flux may be different from that of round tubes or other large tubes. Therefore, studying the characteristics of critical heat flux in rectangular narrow channels is of great significance for engineering applications. Some researchers have conducted experimental research on CHF in rectangular narrow channels and proposed corresponding empirical correlations [5–9]. The empirical correlations are convenient to obtain a reasonable CHF prediction value, but the disadvantage is that they need to be combined with the corresponding experimental working conditions. Once the experimental conditions are exceeded, the applicability of the empirical correlations will be greatly reduced. Therefore, in order to reduce the dependence on experimental data, it is necessary to develop a mechanism model to predict CHF.

Utsuno [10] and Celat [3] develop the theoretical calculation model for CHF, but they are based on round or annular tubes and are not suitable for rectangular narrow channels. Qu [11] develops an annular flow model for predicting the saturated flow boiling heat transfer coefficient for rectangular narrow channels, which can predict well in a large range of flow and heat flux, but it cannot predict liquid film evaporation. Okawa [12] predicts the saturated flow boiling CHF by analyzing the axial change of the liquid film flow velocity in the annular flow region, and it is in good agreement with the experimental data in a wide range. However, when the channel length to channel gap ratio is larger, the predicted value has a large error.

Our research team has conducted extensive experimental and theoretical studies on the CHF and heat transfer characteristics for many years [13–19]. Su [13] proposes a three-fluid model for predicting CHF for annular flow in a double-sided heated vertical annular channel. The model is based on the basic conservation equations, including the mass, momentum and energy conservation equations of the inner and outer liquid film and the momentum conservation equation of the vapor core. Based on above results, Du [20] develops a three-fluid model for predicting CHF of rectangular narrow channels, which is in good agreement with experimental data in a wide range of parameters. However, the model is computationally complex and the prediction accuracy is not enough.

It can be seen from the above introduction that for the critical heat flux, researchers usually use mechanism models or empirical correlations to solve. The mechanism models are derived from the basic theory, and the conclusions are universal. However, additional errors will be introduced due to the lack of certain coefficients in the derivation process. The empirical correlations can be in good agreement with the experimental data, but if it deviates from the applicable range, the prediction effect becomes worse.

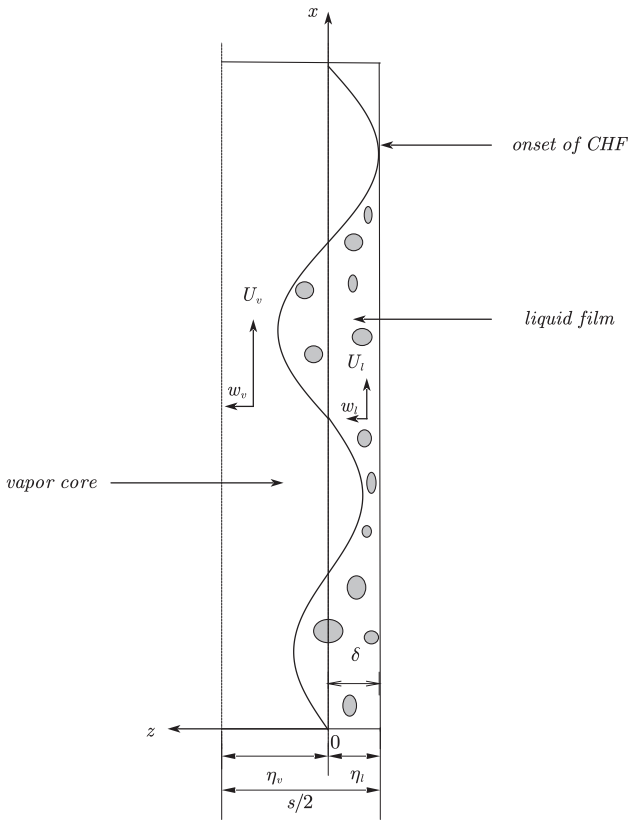

Fig. 2. Schematic diagram of the dryout mechanism model.

The work of this paper combines the advantages of the two methods. The triggering mechanism of the critical heat flux is analyzed theoretically. At the same time, it combines the empirical correlation of the liquid film, so that the unknown coefficients in the theoretical derivation are supported by the experimental data. Meanwhile, the decisive restriction of the experimental conditions on the applicability of the empirical correlation is avoided. Although the work of this paper is based on rectangular narrow channels, it should have applicability to other channels, because the model proposed in this paper is more focused on a method of calculating CHF, which is independent of channel structure type.

2. Dryout mechanism model

2.1. Rectangular channel structure and model assumptions

The schematic diagram of the rectangular channel structure is shown in Fig. 1. In actual, the fluid flows vertically upwards. The length of the channel is *L*, and the flow cross section is a rectangle having a length of *w* and a width of *s*. The fluid is heated by the power applied with a heat flux *q* on both sides of the flow channel. The fluid with a certain degree of subcooling flows into the rectangular channel inlet, and a two-phase flow occurs in the channel with heating. When the flow pattern changes to the annular flow as shown in Fig. 2, the center of the flow channel is the vapor core, and a liquid film attached the flow channel appears. When the heat flux is gradually increased, dryout, namely the critical boiling phenomenon at a high quality, might occur.

The dryout mechanism model schematic is shown in Fig. 2. Since the symmetry of the rectangular channel, Fig. 2 is only the diagram of a half rectangular channel. The following assumptions

are made for the model:

(1) Thicknesses of the liquid film attached to the two heated walls are equal to δ_s, and thicknesses of the liquid film attached to the two unheated walls are equal to δ (δ_s and δ are not equal due to the influence of heating).
(2) The heat dissipation and the heat storage of the rectangular channel wall are not considered in the heating process, that is, the heat applied to the channel is completely absorbed by the fluid.
(3) The dryout phenomenon occurs at the exit of the channel, and the flow pattern at the exit of the channel is an annular flow, that is, the center of the channel is the vapor core, and the liquid film flows along the channel walls.
(4) Dryout is triggered by Kelvin–Helmholtz instability. Sturgis [21] carries out a flow boiling visualization experiment with FC-72 liquid in the rectangular channel (5*2.5 mm cross-section and 101.6 mm heated length). Video images captured at CHF at various flow conditions reveals that vapor coalesces into a series of patches resembling a wavy vapor layer which propagates along the heated wall allowing liquid to contact the wall only at discrete locations. This experimental phenomenon is the physical basis of this hypothesis. When the vapor core velocity and the liquid film velocity couldn't maintain a stable interface wave, the interface wave is diverged, and the wall surface lacks effective wetting of the liquid film, resulting in deterioration of heat transfer and occurrence of dryout.
(5) Both the liquid phase and the vapor phase are non-viscous fluids.

2.2. Mass and energy conservation

According to assumptions 2 and 3, the steam mass flow in the channel when dryout occurs could be expressed as

$$M_v = \frac{2qwL - GswC_{pl}(T_{sat} - T_{in})}{h_{fg}} \tag{1}$$

And then the quality and the liquid film mass flow when dryout occurred are

$$x = \frac{M_v}{Gsw} \tag{2}$$

$$M_l = (1 - x)Gsw \tag{3}$$

The vapor velocity and the liquid film velocity could be respectively obtained by combining the channel geometry shown in Fig. 1

$$U_v = \frac{M_v}{\rho_v(w - 2\delta)(s - 2\delta_s)} \tag{4}$$

$$U_l = \frac{M_l}{\rho_l[sw - (w - 2\delta)(s - 2\delta_s)]} \tag{5}$$

According to Assumption 1

$$\frac{w - 2\delta}{s - 2\delta_s} = \frac{w}{s} \tag{6}$$

Substituting equations (1)–(3), (6) into (4) and (5) respectively, then

$$U_v = \frac{2qwL - GswC_{pl}(T_{sat} - T_{in})}{h_{fg}\rho_v\left(\frac{4s}{w}\delta^2 - 4s\delta + ws\right)} \tag{7}$$

$$U_l = \frac{h_{fg}Gsw - 2qwL + GswC_{pl}(T_{sat} - T_{in})}{h_{fg}\rho_l\left(4s\delta - \frac{4s}{w}\delta^2\right)} \tag{8}$$

2.3. Liquid film thickness calculation

Feind [22] demonstrates that the film thickness of the annular laminar flow could be calculated by the same method as the Nusselt film thickness. Tu [23] uses the liquid film calculation form of Feind in the study of CHF in a round tube, with only changing the empirical constant. When the liquid film thickness of the annular flow is calculated, the same calculation form is used, namely

$$\delta = a_1\left(\frac{3\mu_l^2}{\rho_l^2 g}\right)^{1/3} Re_l^{1/2} \tag{9}$$

The liquid film Reynolds number above is

$$Re_l = \frac{\rho_l U_l \delta}{\mu_l} \tag{10}$$

Substituting equation (10) into (9)

$$\delta = a_2\left(\frac{3\mu_l^2}{\rho_l^2 g}\right)^{2/3}\left(\frac{\rho_l U_l}{\mu_l}\right) \tag{11}$$

where a_2 is the empirical constant for a rectangular channel.

2.4. Kelvin-Helmholtz instability theory

In the region of the annular flow, the interface wave is formed between the vapor and liquid phases, as shown in Fig. 2. The intersection of the liquid film and the entrance of the rectangular channel is taken as the coordinate origin, and the vertical flow direction of the fluid is the positive direction of the x-axis, while the direction from the liquid film to the center of the channel is the positive direction of the z-axis (the y-axis is the direction perpendicular to the paper, and ignore the y-axis direction during the derivation process). In the coordinate system of Fig. 2, the velocity is represented by (u, w). When the annular flow is stable and no interface wave is formed, the vapor phase region is $0 < z < \eta_v$, the liquid phase region is $-\eta_l < z < 0$, and the relationship between η_v and η_l satisfies

$$\eta_v + \eta_l = \frac{s}{2} \tag{12}$$

Based on the coordinate system of Fig. 2, the continuous equations of the vapor and liquid phases can be expressed as

$$\frac{\partial^2\varphi_v}{\partial x^2} + \frac{\partial^2\varphi_v}{\partial y^2} = 0, (0 < z < \eta_v) \tag{13}$$

$$\frac{\partial^2\varphi_l}{\partial x^2} + \frac{\partial^2\varphi_l}{\partial y^2} = 0, (-\eta_l < z < 0) \tag{14}$$

Among them, φ_v represents the velocity potential of steam, φ_l represents the velocity potential of the liquid film.

If the distance from any position on the interface to the x-axis is η, the boundary conditions on the interface corresponding to equations (13) and (14) are

$$\frac{\partial \eta}{\partial t}+U_v\frac{\partial \eta}{\partial x}=w_v,(z=\eta) \tag{15}$$

$$\frac{\partial \eta}{\partial t}+U_l\frac{\partial \eta}{\partial x}=w_l,(z=\eta) \tag{16}$$

The vapor phase velocity at the center satisfies the symmetry condition

$$w_v=0, z=\eta_v \tag{17}$$

The film velocity at the wall satisfies the boundary conditions

$$w_l=0, z=-\eta_l \tag{18}$$

In equations (15) and (16), it is assumed that η meets the following expression

$$\eta=A_0 exp(r_w t+ikx)+C_\eta \tag{19}$$

According to equations (13)–(18), the velocity potential expressions of the vapor phase and the liquid film can be obtained separately

$$\varphi_v=A_v cosh[k(z-\eta_v)]exp(r_w t+ikx)+C_v \tag{20}$$

$$\varphi_l=A_l cosh[k(z+\eta_l)]exp(r_w t+ikx)+C_l \tag{21}$$

The meanings of the above formula are shown in the nomenclature.

Because the relationship between the velocity potential and velocity satisfies

$$\frac{\partial \varphi_v}{\partial x}=U_v,\ \frac{\partial \varphi_v}{\partial z}=w_v \tag{22}$$

$$\frac{\partial \varphi_l}{\partial x}=U_l,\ \frac{\partial \varphi_l}{\partial z}=w_l \tag{23}$$

Substituting equations (20)–(23) into (15) (16) respectively:

$$A_0(r_w+ikU_v)=-kA_v sinh(k\eta_v) \tag{24}$$

$$A_0(r_w+ikU_l)=kA_l sinh(k\eta_l) \tag{25}$$

For general considerations, when the viscous force is considered, the force balance at the position of the phase interface is

$$p_l-p_v=-\sigma\frac{\partial^2\eta}{\partial x^2}+\left(2\mu_l\frac{\partial w_l}{\partial z}-2\mu_v\frac{\partial w_v}{\partial z}\right)+(\rho_l-\rho_v)g\eta \tag{26}$$

The vapor phase pressure term can be obtained based on the equation of motion

$$\rho_v\left(\frac{\partial U_v}{\partial t}+U_v\frac{\partial U_v}{\partial x}\right)=\rho_v g-\frac{\partial p_v}{\partial x}+\mu\nabla\left(\nabla^2\varphi_v\right) \tag{27}$$

According to the continuous equation

$$\nabla^2\varphi_v=0 \tag{28}$$

$$\frac{\partial U}{\partial x}=-\frac{\partial w}{\partial z} \tag{29}$$

Substituting equations (28) and (29) into (27)

$$\rho_v\left(\frac{\partial^2 w_v}{\partial t\partial z}+U_v\frac{\partial^2 w_v}{\partial x\partial z}\right)=\frac{\partial^2 p_v}{\partial x^2} \tag{30}$$

Similarly, the liquid film pressure term satisfies

$$\rho_l\left(\frac{\partial^2 w_l}{\partial t\partial z}+U_l\frac{\partial^2 w_l}{\partial x\partial z}\right)=\frac{\partial^2 p_l}{\partial x^2} \tag{31}$$

Substituting equations (30) and (31) into (26)

$$\rho_l\left(\frac{\partial^2 w_l}{\partial t\partial z}+U_l\frac{\partial^2 w_l}{\partial x\partial z}\right)-\rho_v\left(\frac{\partial^2 w_v}{\partial t\partial z}+U_v\frac{\partial^2 w_v}{\partial x\partial z}\right)$$

$$=-\sigma\frac{\partial^4\eta}{\partial x^4}+\left(2\mu_l\frac{\partial^3 w_l}{\partial x^2\partial z}-2\mu_v\frac{\partial^3 w_v}{\partial x^2\partial z}\right)+(\rho_l-\rho_v)g\frac{\partial^2\eta}{\partial x^2} \tag{32}$$

And substituting equations (19)–(25) into (32) gives a quadratic equation for r_w:

$$R_1 r_w^2+2R_2 r_w+R_3=0 \tag{33}$$

where

$$R_1=\rho_l cosh(k\eta_l)+\rho_v cosh(k\eta_v) \tag{34}$$

$$R_2=R_{2R}+iR_{2I} \tag{35}$$

$$R_{2R}=k^2\mu_l cosh(k\eta_l)+k^2\mu_v cosh(k\eta_v) \tag{36}$$

$$R_{2I}=k\rho_l U_l cosh(k\eta_l)+k\rho_v U_v cosh(k\eta_v) \tag{37}$$

$$R_3=R_{3R}+iR_{3I} \tag{38}$$

$$R_{3R}=-\rho_l k^2 U_l^2 cosh(k\eta_l)-\rho_v k^2 U_v^2 cosh(k\eta_v)+\sigma k^3+(\rho_l-\rho_v)gk \tag{39}$$

$$R_{3I}=2\mu_l k^3 U_l cosh(k\eta_l)+2\mu_v k^3 U_v cosh(k\eta_v) \tag{40}$$

The solution of r_w obtained by equation (33) is

$$r_w=\frac{-R_2\pm\sqrt{R_2^2-R_1R_3}}{R_1} \tag{41}$$

Combined with the research object of this paper and based on assumption 5, formula (41) is written in the complex form with considering the viscosity of the vapor phase and the liquid film both zero

$$r_w=r_{wR}+ir_{wI} \tag{42}$$

$$r_{wR}=\pm\sqrt{\frac{\left(-R_{2I}^2-R_1R_{3R}\right)}{R_1^2}} \tag{43}$$

$$r_{wI}=-\frac{R_{2I}}{R_1} \tag{44}$$

When the complex form of the growth rate r_w has a real part, the instability of the interface wave would increase [24], namely

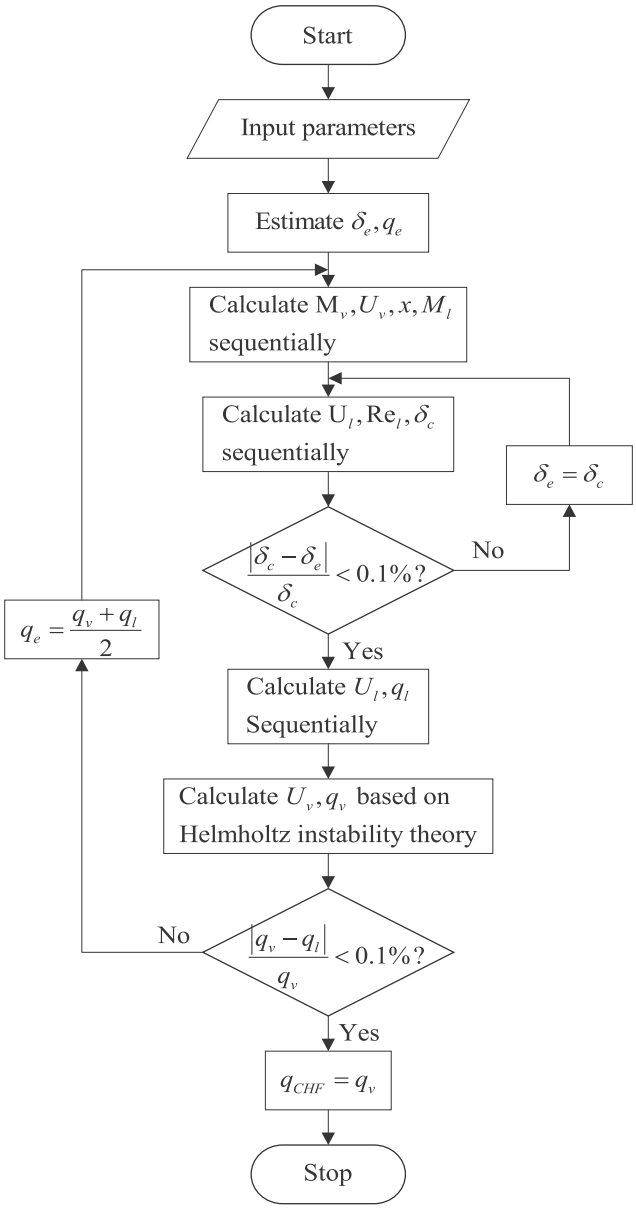

Fig. 3. Flow chart of the model.

$$\frac{-R_{2I}^2 - R_1 R_{3R}}{R_1^2} > 0 \tag{45}$$

When the interface wave is critically stable, the inequality (45) is changed to the equation and (34) ~ (40) are substituted

$$\frac{k\rho_l\rho_v cosh(k\eta_v)cosh(k\eta_l)}{\rho_v cosh(k\eta_v) + \rho_l cosh(k\eta_l)}(U_v - U_l)^2 - \left[\sigma k^2 + (\rho_l - \rho_v)g\right] = 0 \tag{46}$$

Under high pressure conditions, the surface tension is negligible, and the relationship between the vapor phase velocity and the liquid film velocity at critical stability satisfies

$$(U_v - U_l)^2 = \frac{(\rho_l - \rho_v)g}{k}\left[\frac{tanh(k\eta_v)}{\rho_v} + \frac{tanh(k\eta_l)}{\rho_l}\right] \tag{47}$$

Referring to the assumption of Wallis [25], it could be considered that the wave number is small when the interface wave is critically stable, that is $k\eta_v \ll 1$, $k\eta_l \ll 1$. According to the nature of the hyperbolic tangent function, formula (47) could be expressed as

$$(U_v - U_l)^2 = \left(\frac{\eta_v}{\rho_v} + \frac{\eta_l}{\rho_l}\right)(\rho_l - \rho_v)g \tag{48}$$

When the interface wave is critically stable, the vapor phase velocity expression is

$$U_v = U_l + \sqrt{\left(\frac{\eta_v}{\rho_v} + \frac{\eta_l}{\rho_l}\right)(\rho_l - \rho_v)g} \tag{49}$$

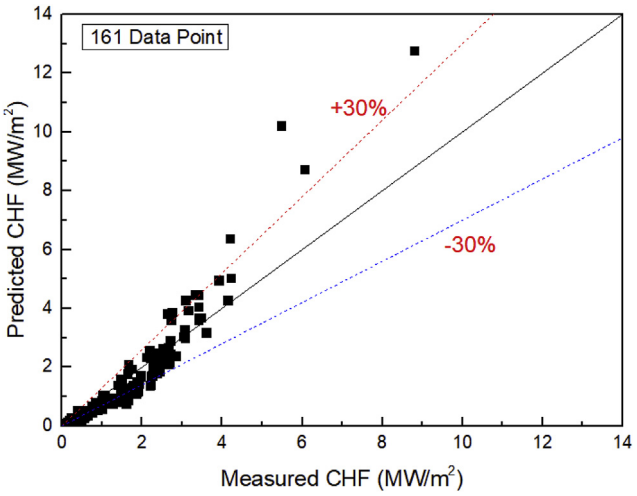

Fig. 4. Comparison of predicted and experimental values.

2.5. CHF calculation

According to equation (7), an expression for determining the heat flux based on the vapor phase velocity could be obtained

$$q_v = \frac{U_v h_{fg}\rho_v\left(\frac{4s}{w}\delta^2 - 4s\delta + ws\right) + GswC_{pl}(T_{sat} - T_{in})}{2wL} \tag{50}$$

An expression for obtaining a heat flux based on the liquid film velocity could be obtained from formula (8)

$$q_l = \frac{GswC_{pl}(T_{sat} - T_{in}) + h_{fg}Gsw - U_l h_{fg}\rho_l\left(4s\delta - \frac{4s}{w}\delta^2\right)}{2wL} \tag{51}$$

q_l is the heat flux obtained from the liquid film velocity under the condition of liquid film thickness convergence. q_v is the heat flux obtained from the vapor phase velocity under the critical stability condition of the Kelvin–Helmholtz interface wave. For the same case, q_l and q_v should be equal, and the heat flux is calculated iteratively until convergence. At this time, since the critical stability condition of the Kelvin–Helmholtz interface wave is satisfied, according to assumption 4, it is considered that the dryout occurs.

The CHF calculation process in the rectangular narrow channel when dryout occurs is as follows.

1. Enter the geometric parameters and thermal parameters of the rectangular narrow channel.
2. Set initial liquid film thickness and initial heat flux.

Table 1
Range of experimental data in literatures.

Author	Jacket [26]	Tippets [27]	Mishima [28]
Pressure (MPa)	13.79	6.9	0.1
Mass flux (kg/m^{2}s)	231.9–4462	244–1940	10–7500
Inlet subcooling (K)	4.4–186.1	7–93	40–80
L (mm)	306.4–685.8	940	98
w (mm)	25.4	53	40
s (mm)	1.27–2.46	6.4–12.7	1.0–2.0

3. Calculate vapor phase mass flow, vapor phase velocity, quality and liquid film mass flow.
4. Calculate liquid film velocity, liquid film Reynolds number and liquid film thickness.
5. Determine whether the thickness of the liquid film converges. If there is no convergence, the thickness of the liquid film is taken as a new calculated value and return to the fourth step.
6. Recalculate the liquid film velocity and the corresponding heat flux q_l according to the converging liquid film thickness.
7. Calculate the vapor phase velocity and the corresponding heat flux q_v according to the Kelvin–Helmholtz critical stability condition.
8. Determine whether q_l and q_v are equal. If they are not equal, take the mean value as the new heat flux value and return to the third step.
9. When q_l and q_v are equal, q_v is the CHF value under the corresponding operating condition.

The calculation flow chart is shown in Fig. 3.

3. Experiment validation of the models

In order to verify the correctness of the dryout model, the experimental data are used. Since the existing research on the rectangular narrow channel is not as rich as the round tube, there is small number of CHF experimental data of the rectangular narrow channel. In this paper, 161 sets of rectangular narrow channel CHF experimental data from Jacket [26], Tippets [27] and Mishima [28] are selected to verify the dryout model Table 1.

The model calculation results and experimental results are shown in Fig. 4.

For the selected 161 sets of experimental data, the predicted value of the model proposed in this paper is about ±30%. CHFR represents the ratio of the calculated value of the CHF model to the experimental value. The expression of CHFR and its mean are calculated as follows

$$\mathrm{CHFR} = \frac{q_{c,cal}}{q_{c,exp}} \tag{52}$$

$$\mu_{CHFR} = \frac{1}{N}\sum_{i=1}^{N} CHFR_i \tag{53}$$

The model calculation error and the average value of CHFR satisfy

$$\mathrm{err}_{model} = 1 - \mu_{CHFR} \tag{54}$$

For different pressure ranges, the error analysis of the model is shown in Table 2.

As can be seen from Table 2, the model proposed in this paper has better applicability under high pressure conditions.

Combining Fig. 4 and Table 2, it can be seen that the model proposed in this paper has certain accuracy for CHF prediction under high pressure conditions, which proves that this new calculation method is feasible.

For model validation, this article is relatively simple for two reasons.

1. Limited experimental data are available. The CHF experiments under high pressure conditions of rectangular narrow channels are difficult, and the experimental data obtained from the published literature are limited.
2. Even publicly available experimental data does not provide comprehensive parameters for model validation. In order to verify the correctness of the model in this paper, in addition to the CHF value, liquid film thickness, vapor phase velocity, liquid phase velocity, and void fraction are all important parameters. However, in the relevant literature of CHF experiments, only the operating parameters (pressure, mass flow rate, inlet subcooling, channel size, etc.) and CHF value under the corresponding operating conditions are provided, which brings further difficulties to the model validation in this paper.

Based on the above two reasons, the evaluation of the accuracy of the model in this paper will be the next step for the authors. The authors consider conducting visualization CHF experiments under high pressure in the future. With the help of visualization and image processing technology, the key parameters such as liquid film thickness and void fraction are obtained to verify various parameters in the model in this paper, not just the final CHF value.

However, from the perspective of engineering application, the ultimate goal of CHF research is to propose a method to obtain the predicted CHF value, so as to avoid the occurrence of CHF phenomenon in the actual thermal hydraulic operation process. Fig. 4 has proved that the model proposed in this paper is valuable for engineering application.

4. Conclusions

In this paper, a dryout mechanism model is established. The Kelvin–Helmholtz instability is used as the criterion for the occurrence of dryout. The expression of vapor phase velocity at the time of dryout is derived, and the empirical correlation of liquid film thickness is introduced. In the actual situation, when the dryout phenomenon occurs, the CHF value obtained from the liquid film thickness should be the same as the CHF value obtained according to the Kelvin–Helmholtz critical stability. Therefore, the convergent CHF value could be obtained by iteratively calculating.

Comparing with the experimental data, the average error of the model is −15.4% with the 95% confidence interval [-20.5%, −10.4%], illustrating that this mechanism model is suitable for the pressure

Table 2
Error analysis under different pressure ranges.

Pressure (MPa)	CHFR		Model error	
	Average value	95% confidence interval	Average value	95% confidence interval
0.1–13.79	0.789	[0.739, 0.839]	−21.1%	[-26.1%, −16.1%]
6.89–13.79	0.846	[0.795, 0.896]	−15.4%	[-20.5%, −10.4%]

range of 6.89–13.79 MPa. Pressure has a decisive influence on the prediction accuracy of this model. This is because the model is based on the assumption of high-pressure conditions, such as ignoring the influence of surface tension under high pressure conditions, making the model more suitable for high pressure conditions.

The proposed and validated dryout mechanism model greatly reduces the dependence on experimental data and avoids using empirical correlations to predict CHF. It is of great significance for the study of CHF in rectangular narrow channels.

Declaration of competing interest

The authors declare that we do not have any commercial or associative interest that represents a conflict of interest in connection with the work submitted.

Acknowledgement

The authors gratefully acknowledge the supports from Natural Science Foundation of China (Grant No. 11675127) and K. C. Wong Education Foundation.

Nomenclature and units

A_0, A_v, A_l	complex amplitudes
a_1, a_2	Empirical coefficient
C_{pl}	Liquid phase constant pressure specific heat, $J/\ (kg \cdot K)$
C_η, C_v, C_l	complex conjugate of the preceding expression
De	Channel hydraulic diameter, m
G	Mass flow rate, $kg/(m^2 \cdot s)$
g	Gravity acceleration, m/s^2
h_{fg}	Latent heat of vaporization, J/kg
i	Imaginary unit, $\sqrt{-1}$
k	Wave number
L	Channel length, m
M_l	Liquid phase mass flow, kg/s
M_v	Vapor phase mass flow, kg/s
p	System pressure, MPa
p_l	Liquid phase pressure, MPa
p_v	Vapor phase pressure, MPa
q	Heat flux, W/m^2
q_{CHF}	Critical heat flux, W/m^2
q_e	Estimated value of q, W/m^2
q_l	Heat flux calculated from liquid film thickness, $W/\ m^2$
q_v	Heat flux calculated from vapor phase velocity, $W/\ m^2$
R_1, R_2, R_3	Coefficients on the quadratic equation of r_w
R_{2R}, R_{2I}	Real and imaginary parts of R_2
R_{3R}, R_{3I}	Real and imaginary parts of R_3
Re_l	Liquid film Reynolds number
r_w	complex growth rate
r_{wR}, r_{wI}	Real and imaginary parts of r_w
s	Rectangular section width, m
T_{in}	Inlet fluid temperature, K
T_{sat}	Saturating temperature, K
U_l	Liquid phase velocity along the flow direction, $m/\ s$
U_v	Vapor phase velocity along the flow direction, $m/\ s$
w	Rectangular section length, m
w_l	Liquid phase velocity along the direction perpendicular to the flow direction, m/s
w_v	Vapor phase velocity along the direction perpendicular to the flow, m/s
x	Quality
δ	Liquid film thickness attached to the short side of the rectangular section, m
δ_c	Calculated value of δ, m
δ_e	Estimated value of δ, m
δ_s	Liquid film thickness attached to the long side of the rectangular section, m
η	The distance from any position of the interfacial wave to the x-axis, m
η_l	Average film thickness, m
η_v	The distance from the average thickness of the liquid film to the center of the channel, m
μ_l	Liquid phase dynamic viscosity, $Pa \cdot s$
μ_v	Vapor phase dynamic viscosity, $Pa \cdot s$
ρ_l	Liquid phase density, kg/m^3
ρ_v	Vapor phase density, kg/m^3
σ	Surface tension, N/m
φ_l	Liquid phase velocity potential
φ_v	Vapor phase velocity potential

Appendix A. Supplementary data

Supplementary data to this article can be found online at https://doi.org/10.1016/j.net.2020.03.018.

References

[1] J. Huang, Y. Huang, Q. Wang, et al., Numerical study on effect of gap width of narrow rectangular channel on critical heat flux enhancement, Nucl. Eng. Des. 239 (2) (2009) 320–326.
[2] L. Li, D. Fang, D. Zhang, et al., Flow and heat transfer characteristics in plate-type fuel channels after formation of blisters on fuel elements, Ann. Nucl. Energy 134 (2019) 284–298.
[3] G.P. Celata, K. Mishima, G. Zummo, Critical heat flux prediction for saturated flow boiling of water in vertical tubes, Int. J. Heat Mass Tran. 44 (22) (2001) 4323–4331.
[4] T. Okawa, A. Kotani, I. Kataoka, et al., Prediction of the critical heat flux in annular regime in various vertical channels, Nucl. Eng. Des. 229 (2–3) (2004) 223–236.
[5] Y. Sudo, M. Kaminaga, A CHF characteristic for downward flow in a narrow vertical rectangular channel heated from both sides, Int. J. Multiphas. Flow 15 (5) (1989) 755–766.
[6] Y. Sudo, M. Kaminaga, A new CHF correlation scheme proposed for vertical rectangular channels heated from both sides in nuclear research reactors, J. Heat Tran. 115 (2) (1993) 426–434.
[7] Y. Sudo, Study on critical heat flux in rectangular channels heated from one or both sides at pressures ranging from 0.1 to 14 MPa, J. Heat Tran. 118 (3) (1996) 680–688.
[8] Y. Sudo, M. Kaminaga, Critical heat flux at high velocity channel flow with high subcooling, Nucl. Eng. Des. 187 (2) (1999) 215–227.
[9] D. Lu, X. Bai, Y. Huang, et al., Study on CHF in thin rectangular channels and evaluation of its empirical correlations, Chin. J. Nucl. Sci. Eng. 24 (3) (2004) 242–248.
[10] H. Utsuno, F. Kaminaga, Prediction of liquid film dryout in two-phase annular-mist flow in a uniformly heated narrow tube development of analytical method under BWR conditions, J. Nucl. Sci. Technol. 35 (9) (1998) 643–653.
[11] W. Qu, I. Mudawar, Flow boiling heat transfer in two-phase micro-channel heat sinks––II. Annular two-phase flow model, Int. J. Heat Mass Tran. 46 (15) (2003) 2773–2784.
[12] T. Okawa, A. Kotani, I. Kataoka, et al., Prediction of the critical heat flux in annular regime in various vertical channels, Nucl. Eng. Des. 229 (2–3) (2004) 223–236.
[13] G. Su, J. Gou, S. Qiu, et al., Theoretical calculation of annular upward flow in a narrow annuli with bilateral heating, Nucl. Eng. Des. 225 (2–3) (2003) 219–247.
[14] F.A.N. Pu, Q.I.U. Sui-Zheng, J.I.A. Dou-Nan, An investigation of flow characteristics and critical heat flux in vertical upward round tube, Nucl. Sci. Tech. 17 (3) (2006) 170–176.
[15] G. Su, K. Fukuda, D. Jia, et al., Application of an artificial neural network in reactor thermohydraulic problem: prediction of critical heat flux, J. Nucl. Sci. Technol. 39 (5) (2002) 564–571.
[16] Y.W. Wu, G.H. Su, S.Z. Qiu, et al., Experimental study on critical heat flux in bilaterally heated narrow annuli, Int. J. Multiphas. Flow 35 (11) (2009) 977–986.
[17] R. Sun, G. Song, D. Zhang, et al., Experimental study of single-phase flow and heat transfer in rectangular channels under uniform and non-uniform heating, Exp. Therm. Fluid Sci. (2020) 110055.
[18] G. Song, D. Zhang, G.H. Su, et al., Assessment of ECCMIX component in RELAP5 based on ECCS experiment, Nucl. Eng. Technol. 52 (1) (2019) 59–68.
[19] G. Song, D. Zhang, Q. Liu, et al., RELAP5/MOD3. 4 calculation and model

evaluation based on upper plenum entrainment experiment in AP1000, Ann. Nucl. Energy 138 (2020) 107143.
[20] D.X. Du, W.X. Tian, G.H. Su, et al., Theoretical study on the characteristics of critical heat flux in vertical narrow rectangular channels, Appl. Therm. Eng. 36 (2012) 21–31.
[21] J.C. Sturgis, I. Mudawar, Critical heat flux in a long, rectangular channel subjected to one-sided heating—I. Flow visualization, Int. J. Heat Mass Tran. 42 (10) (1999) 1835–1847.
[22] F. Feind, Falling liquid films with countercurrent air flow in vertical tubes, VDI-Forschungscheft 481 (1960) 5–35.
[23] K.C. Tu, C.H. Lee, S.J. Wang, et al., A new mechanistic critical heat flux model at low-pressure and low-flow conditions, Nucl. Technol. 124 (3) (1998) 243–254.
[24] T. Funada, D.D. Joseph, Viscous potential flow analysis of Kelvin–Helmholtz instability in a channel, J. Fluid Mech. 445 (2001) 263–283.
[25] G.B. Wallis, J.E. Dodson, The onset of slugging in horizontal stratified air-water flow, Int. J. Multiphas. Flow 1 (1) (1973) 173–193.
[26] H.S. Jacket, J.D. Roarty, J.E. Zerbe, Investigation of Burnout Heat Flux in Rectangular Channels at 2000 Psia, Westinghouse Electric Corp. Bettis Plant, Pittsburgh, 1956.
[27] F.E. Tippets, Critical Heat Flux and Flow Pattern Characteristics of High Pressure Boiling Water in Forced Convection, General Electric Co. Atomic Power Equipment Dept., San Jose, Calif., 1962.
[28] K. Mishima, F. Tanaka, T. Hibiki, et al., Heat transfer study for thermal-hydraulic design of the solid-target of spallation neutron source, J. Nucl. Sci. Technol. 38 (10) (2001) 832–843.